RSC Advances

PAPER

View Article Online
View Journal | View Issue



Cite this: *RSC Adv.*, 2024, **14**, 33764

# Fabrication of monodisperse micron-sized and aldehyde-functionalized microspheres coating with covalent organic framework for efficient and rapid removal of copper ions from wastewater†

Xiaoqiong Wang,[a] Qingyan Bai,[a] Mingjia Yan,[a] Yashuai Zhao,[a] Shujuan Ma,[c] Chunmiao Bo *[a] and Junjie Ou *[bc]

Covalent organic frameworks (COFs) possess an excellent ability for absorbing heavy metals, but their uneven particle size, difficult separation, and poor dispersion limit their wide application in the treatment of heavy metal pollution. In this paper, a monodisperse poly(4-allyloxybenzaldehyde-*co*-divinylbenzene) microsphere (denoted as PAD) was prepared with 4-allyloxybenzaldehyde as a functional monomer and divinylbenzene (DVB) as a crosslinker by one-step seed swelling polymerization. Subsequently, oxalyldihydrazide (ODH) and 2,4,6-trihydroxybenzene-1,3,5-tricarbaldehyde (Tp) were chosen as the precursors for coating the COF layer onto the surface of PAD through a one-pot method. The resulting monodisperse particles (diameter = 6.3 μm) with a core–shell structure were assigned as **PAD@COF** and possessed excellent dispersibility in water along with a high specific surface area of 163.8 $m^2\ g^{-1}$. In isothermal and dynamic adsorption experiments, the maximum adsorption capacity of $Cu^{2+}$ reached 270.9 mg $g^{-1}$, with the adsorption amount reaching 93 mg $g^{-1}$ after only 10 min. The Langmuir isothermal adsorption model and pseudo-second-order kinetic model were consistent with the adsorption process, indicating that the adsorption of $Cu^{2+}$ on **PAD@COF** occurred as a monolayer and that the adsorption process was controlled by chemical processes.

Received 11th August 2024
Accepted 10th October 2024

DOI: 10.1039/d4ra05820h

rsc.li/rsc-advances



## 1 Introduction

Covalent organic frameworks (COFs), as porous materials constructed by the covalent bonds of organic units, were originally discovered in 2005.[1] Due to their high specific surface area, controllable pore structure, and surface functionalization,[2] COFs exhibit a wide range of application prospects in many fields such as gas adsorption and separation,[3] energy storage,[4] catalysis,[5] desalination,[6] sensing,[7] detection,[8] photoelectric applications[9] and environmental purification.[10] The highly interconnected structure of COFs provides a robust foundation for the development of adsorption materials with exceptional selectivity and superior adsorption properties. In recent years, COFs have been widely utilized in water remediation,[11] organic pollutant adsorption,[12] electrocatalysis,[13] photocatalysis and other fields,[14,15] and their synthesis has also been investigated.[16,17] However, most current COF materials involve two-dimensional structures[18] and lack regular morphology,[19] making the molding problem of COF materials a significant challenge.

The size and shape of COF components cannot be controlled under solvothermal conditions, often resulting in mixed shapes and grain sizes that are difficult to separate.[20] A few microspheres or particles with controllable morphology were synthesized as the core, and then the COF layer was integrated onto the surfaces of these microspheres, thus improving the controllable morphology of COFs. For example, Gao *et al.* took $Fe_3O_4$ as the core and then made surface modifications for the selective enrichment of hydrophobic peptides.[21] Xu and co-workers reported a core–shell composite of COF material grown on the surface of aminopropyl-functionalized $SiO_2$ microspheres for enantiomeric separation by high-performance liquid chromatography.[22] Additionally, the direct preparation method of spherical COF materials was developed. Ma and colleagues selected 2,5-divinylterephthalaldehyde and 1,3,5-tris(4-aminophenyl)benzene as precursors dissolved in acetonitrile and then added acetic acid at room temperature to synthesize a micron-scale spherical COF for the selective enrichment of hydrophobic peptides.[23] Recently, Zhu

[a]*School of Chemistry and Chemical Engineering, Ningxia Key Laboratory of Solar Chemical Conversion Technology, Key Laboratory for Chemical Engineering and Technology, State Ethnic Affairs Commission, North Minzu University, Yinchuan, 750021, China. E-mail: bocm-001@163.com; Fax: +86-0951-2067917; Tel: +86-0951-2067917*

[b]*College of Chemistry and Materials Science, Northwest University Xi'an, 710127, China. E-mail: junjieou@nwu.edu.cn; junjieou@dicp.ac.cn; Fax: +86-29-81535026; Tel: +86-29-81535026*

[c]*CAS Key Laboratory of Separation Science for Analytical Chemistry, Dalian Institute of Chemical Physics, Chinese Academy of Sciences, Dalian 116023, China*

† Electronic supplementary information (ESI) available. See DOI: https://doi.org/10.1039/d4ra05820h

*et al.* developed a polymerization-induced phase separation method for the controlled synthesis of imine-linked polymers, which was then crystallized to produce monolithic COF, expanding a new avenue for shape-controlled COF synthesis.[24] More recently, Xu *et al.* successfully prepared surface-functionalized COF microspheres by the *in situ* linker exchange and applied them as stationary phase for chiral chromatography to achieve effective enantioseparation.[25] However, these synthetic approaches of spherical or monolithic COF have not been widely applied, and the difficulty of synthesis should not be underestimated. At present, the organization of three-dimensional COF synthesis often involves secondary phases (polymers, silica, *etc.*) to provide templates or supports to stabilize the structure.[26] In addition, because of the covalent mechanism of the synthesis process, many core–shell structured materials are irreversible once the reaction is carried out, and the materials lack reusable characteristics and are environmentally hazardous; thus, the recycling of materials is also a major focus of our attention. It is well known that the imide bond is a covalent bond formed by the condensation reaction of the aldehyde group and amino group, which contains certain reversibility.[27] Under mild conditions, the imine bond can be hydrolyzed, resulting in the decomposition of the product into aldehyde and amino groups. This reversibility allows imine bonds to play an important role in some biochemical reactions and organic synthesis, facilitating the degradation or breakdown of materials into their original functional groups.

Herein, we selected 4-allyloxybenzaldehyde, a functional monomer containing an aldehyde group, to prepare micron-scale monodisperse microspheres by one-step seeded swelling polymerization. Subsequently, 2,4,6-trihydroxybenzene-1,3,5-tricarbaldehyde (Tp) and oxalyldihydrazide (ODH) were selected to generate porous COF, which was grafted onto the surface of PAD through a one-pot method and named as **PAD@COF**. The novel composite **PAD@COF** not only improves the preparation efficiency of COF materials but also provides a new possibility for its application in adsorption separation and other aspects.

# 2 Experimental section

## 2.1 Reagents and materials

4-Allyloxybenzaldehyde (97%) was obtained from Alfa Aesar (Shanghai, China). Dibutyl phthalate (DBP), Tp and acetic acid were from Innochem (Beijing, China). Azodiisobutyronitrile (AIBN), styrene (St), divinylbenzene (DVB), polyvinyl alcohol (PVA), sodium dodecyl sulfate (SDS), ODH and *n*-butanol were purchased from Aladdin (Shanghai, China). Toluene and anhydrous ethanol were acquired from Beilian Fine Chemicals Development (Tianjin, China). Tetrahydrofuran (THF) was supplied by Jinshan Chemical Reagent (Chengdu, China). Other chemical reagents were of analytical grade.

## 2.2 Synthesis of monodisperse poly(4-allyloxybenzaldehyde-*co*-divinylbenzene) microspheres

According to a previous report,[28] polystyrene seeds were synthesized *via* dispersion polymerization. Monodisperse poly(4-allyloxybenzaldehyde-*co*-divinylbenzene) microspheres were synthesized by one-step seeded swelling polymerization using 4-allyloxybenzaldehyde as a functional monomer and DVB as the crosslinking agent. Typically, a certain volume of polystyrene seeds was placed in a round-bottomed flask for swelling at room temperature, followed by a certain volume of the water phase (SDS and PVA). After that, the oil phase was configured with a certain volume of 4-allyloxybenzaldehyde, DVB, toluene, DBP, and cyclohexanol, and AIBN was added and sonicated until it dissolved completely. The water and oil phases were mixed uniformly through ultrasonication until emulsification was completed and there were no oil droplets on the surface. The resultant solution, after cell disruption, was poured into a flask, sealed under nitrogen protection, and swollen at 25 °C for 24 h at a mechanical speed of 100 rpm, and then reacted at 70 °C for 24 h. After washing, the monodisperse poly(4-allyloxybenzaldehyde-*co*-divinylbenzene) microspheres were acquired and denoted as PAD.

## 2.3 Surface modification of poly(4-allyloxybenzaldehyde-*co*-divinylbenzene) microspheres with the COF layer

Based on our previous result,[29] ODH and Tp were selected as surface-modified monomers for monodisperse polymer microspheres. The monomer material with amine and aldehyde groups was grafted onto the surface of PAD. In brief, 36 mg ODH was added into 10 mL water and dispersed evenly by ultrasonication. Then, 42 mg Tp was weighed and placed in a mixture of 2.4 mL toluene, *n*-butanol, and glacial acetic acid (v/v/v = 5/5/2) and ultrasonically dispersed. Then, 135 mg monodisperse PAD was placed in 5 mL water for ultrasonic dispersion, and the condensation reflux reaction was carried out at 120 °C by magnetic agitation for 24 h. After the precipitate was centrifuged with THF and anhydrous ethanol two times, the washed solid precipitate was freeze-dried for 12 h, and the dried powder products were collected and weighed for preservation. The dried product was denoted as **PAD@COF**.

For comparison, an ampoule bottle of dimensions 10 mm (o.d.) × 5 mm (i.d.) was filled with ODH (36 mg), Tp (42 mg), 0.5 mL of anhydrous dioxane and 0.5 mL of glacial acetic acid. After ultrasonic dispersion for 30 min and sealing with a flame, the reactants were heated at 120 °C for 48 h. The washed and dried product was denoted as COF.

## 2.4 Evaluation of reusability

The cyclic stability of the material was assessed through adsorption–desorption experiments by ultrasonically washing the adsorbed material with 0.1 mol $L^{-1}$ HCl, drying the precipitate, and reusing it for copper ion adsorption under the same conditions for 10 cycles.

## 2.5 Determination of PAD@COF in real samples

The adsorption capability of **PAD@COF** for $Cu^{2+}$ in actual samples was measured. Lake water (Ming Lake, Yinchuan, China) was chosen as the sample. After centrifugal, filtration and the addition of $Cu^{2+}$, a water sample containing $Cu^{2+}$ (3.5 mg $L^{-1}$) was obtained. Then, 8 mg of **PAD@COF** were mixed

with 100 mL of this water sample. After shaking at room temperature for 1 h, the supernatant was collected to measure the concentration of $Cu^{2+}$ and calculate the adsorption amount.

# 3 Results and discussion

## 3.1 Design and synthesis of monodisperse aldehyde-functionalized microspheres (PAD)

A monomer of 4-allylbenzaldehyde containing an aldehyde group was selected to synthesize monodisperse microspheres by a one-step seed swelling polymerization method. Given the reversible imine bonds, the synthesized microspheres containing the aldehyde group were expected to integrate with the COF-containing terminal amine group to synthesize core–shell COF microspheres, as shown in Fig. 1. Due to the reversible condensation reaction between the amino group and the aldehyde group, the imine bond can be hydrolyzed for suitable degradation so that the product can be decomposed into the aldehyde group and the amino group again. Therefore, the resulting microspheres are green and environment friendly and can be reused.

In this case, polystyrene seeds were successfully prepared *via* dispersion polymerization. The polystyrene seed exhibited outstanding monodispersity and smooth surface characteristics, and the average diameter of seed particle size was about 3 μm (Fig. S1†). To begin with, the oil phase consisted of 4-allyloxybenzaldehyde, DVB, and porogenic solvents, while the aqueous solution contained 5% PVA and 0.2% SDS. After the swelling and polymerization reaction, the resulting PAD resins with different morphologies were successfully prepared. Eventually, the mass ratio of the seed to the total monomers, the molar ratio of the monomer to the crosslinker, different binary porogenic systems (DBP-toluene system, toluene–cyclohexanol system, and DBP–cyclohexanol system) and the ratio of the oil–water phase on the resin morphology were carefully investigated, and the specific synthetic parameters are listed in Table 1.

**3.1.1 Effect of the binary porogenic system (DBP–toluene) on the morphologies of PAD.** Polar solvent DBP and non-polar solvent toluene were initially selected as binary porogenic agents. The effects of the polystyrene seed dosage, the monomer/crosslinker (*n*/*n*) and the ratio of oil to water on the size and morphology of the particles were investigated.

When the monomer/crosslinker (*n*/*n*) was almost 1 : 1, the amount of polystyrene seed was 233 mg, and the oil–water volume ratio was maintained at 3 : 25. As presented in Fig. 2a, **PAD-1** with a broken spherical shape was generated, only a few retained the spherical structures with a particle size of 2.4 μm, and the final yield was only 7.0%. The mass ratio of the seed/total monomers remained 3 : 10, **PAD-2** possessed a spherical shape but a few small particles adhered on its surface and gave uneven morphology, the particle size of the sphere was 6.9 μm (Fig. S2a†), and the yield was only 6.6%. It was inferred that the seeds could not fully absorb the oil phase due to the reduction of the seed amount, and the self-polymerization of the excess crosslinking agent and monomer would produce more small particles. The following experiments were attempted to be improved by changing the proportion of the functional monomer and crosslinker. When the amount of functional monomer to crosslinker was 7 : 5, the surface adhesion of **PAD-3** was reduced but the shape was not uniform, as depicted in Fig. S2b.† The self-polymerization of the functional monomer and crosslinker occurred around the product; nevertheless, the yield increased significantly to 30.7%. When monomer/crosslinker (*n*/*n*) was almost 1 : 1, the resulting **PAD-4** was uniformly spherical. However, compared to the initial polystyrene seeds (Fig. S1†), the microsphere size was only 2.6 μm (Fig. S2c†), indicating that the seeds did not expand successfully. The oil phase cannot be completely absorbed due to the lack of the water phase, and most of the resins are self-

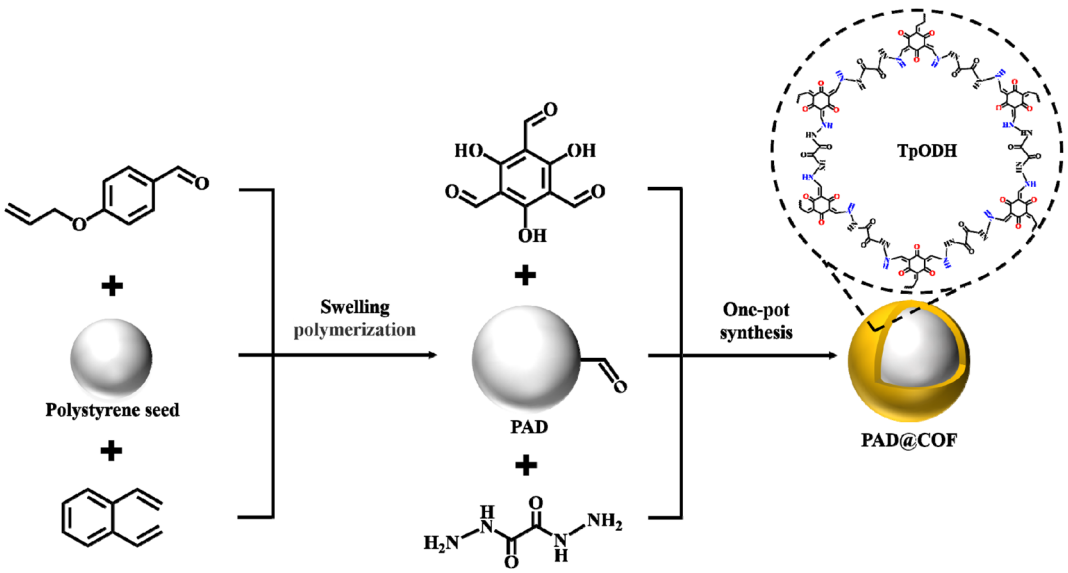


Fig. 1 Schematic preparation of PAD@COF.

Table 1 Effects of binary porogenic agents on the morphology of poly(4-allyloxybenzaldehyde-*co*-DVB) particles[a]

| Materials | Seed/total monomers (mg/mg) | Monomer/cross-linking agent (*n*/*n*) | Porogenic agent system (v/v) | Oil/water (v/v) | Size (μm) | Productivity (%) |
|---|---|---|---|---|---|---|
| **PAD-1** | 1 : 2 | 1 : 1 | DBP : toluene | 3 : 25 | 2.4 | 7.0 |
| **PAD-2** | 3 : 10 | 1 : 1 | DBP : toluene | 3 : 25 | 6.9 | 6.6 |
| **PAD-3** | 3 : 10 | 7 : 5 | DBP : toluene | 3 : 25 | 6.1 | 30.7 |
| **PAD-4** | 3 : 10 | 1 : 1 | DBP : toluene | 3 : 25 | 2.6 | 55.1 |
| **PAD-5** | 3 : 10 | 1 : 1 | DBP : toluene | 3 : 50 | 7.2 | 26.5 |
| **PAD-6** | 3 : 10 | 1 : 1 | DBP : toluene | 3 : 50 | 5.5 | 42.8 |
| **PAD-7** | 2 : 5 | 1 : 1 | DBP : toluene | 3 : 50 | 6.8 | 37.5 |
| **PAD-8** | 1 : 2 | 1 : 1 | DBP : toluene | 3 : 50 | — | 41.9 |
| **PAD-9** | 3 : 10 | 1 : 1 | Toluene : cyclohexanol | 3 : 50 | 5.9 | 19.9 |
| **PAD-10** | 3 : 5 | 1 : 1 | Toluene : cyclohexanol | 3 : 50 | 5.9 | 14.9 |
| **PAD-11** | 1 : 2 | 1 : 1 | Toluene : cyclohexanol | 3 : 50 | 5.4 | 18.9 |
| **PAD-12** | 3 : 10 | 1 : 1 | Toluene : cyclohexanol | 3 : 50 | 7.1 | 33.2 |
| **PAD-13** | 1 : 3 | 1 : 1 | Toluene : cyclohexanol | 3 : 50 | 6.6 | 35.3 |
| **PAD-14** | 2 : 5 | 1 : 1 | Toluene : cyclohexanol | 3 : 50 | — | 9.5 |
| **PAD-15** | 1 : 2 | 1 : 1 | DBP : cyclohexanol | 3 : 50 | 5.1 | 21.4 |
| **PAD-16** | 1 : 2 | 1 : 1 | DBP : cyclohexanol | 3 : 50 | 6.2 | 39.5 |
| **PAD-17** | 3 : 5 | 3 : 2 | DBP : cyclohexanol | 3 : 50 | 6.4 | 39.2 |
| **PAD-18** | 1 : 2 | 2 : 1 | DBP : cyclohexanol | 3 : 50 | 6.3 | 35.6 |

[a] In these cases, the volume ratio of binary porogenic agents (DBP/toluene, toluene : cyclohexanol, DBP : cyclohexanol) was 1 : 1. "—" indicates uneven size. For **PAD-12**, five times the amount was added compared to **PAD-9**, and similarly, for **PAD-16** compared to **PAD-15**.

polymerized precursors. As a result, the oil–water volume ratio was changed to 3 : 50 and the monomer/crosslinker (*n*/*n*) was almost 1 : 1. As depicted in Fig. S2d,† the prepared **PAD-5** resin exhibited a uniform spherical structure, but the particle size of the spherical resin reached 7.2 μm, and the final yield was 26.5%. Subsequently, the amount of polystyrene seed was doubled (**PAD-6**), the size of the acquired microspheres was reduced to 5.5 μm (Fig. 2b), the product adhesion slowed down, but the surface of the microspheres became rougher, whose yield reached 42.8%. By changing the total amount of monomers (4-allyloxybenzaldehyde and DVB), the acquired **PAD-7** (Fig. S2e†) and **PAD-8** (Fig. S2f†) were not satisfactory. In short, these results demonstrated that the DBP–toluene system is not suitable for the fabrication of the PAD spheres.

**3.1.2 Effect of binary porogenic system (toluene–cyclohexanol) on the morphologies of PAD.** To further investigate the effect of porogenic agents on PAD morphology, polar cyclohexanol and non-polar toluene were selected as the binary porogenic agents. The oil-water ratio of the whole system was 3 : 50, and the morphology of the product was controlled by changing the dosage of polystyrene seeds or the monomer/crosslinker (*n*/*n*). **PAD-9** was obtained with the monomer/crosslinker (*n*/*n*) ratio of almost 1 : 1, when the volume ratio of cyclohexanol/toluene was 1 : 1 and the dosage of polystyrene seed was 155 mg. As shown in Fig. S3a,† the prepared spherical resin exhibited good monodispersity, particle size of 5.9 μm and yield of 19.9%, but the surface was rough. Adjusting the mass ratio of seed/total monomers at 3 : 5 (**PAD-10**), the resin possessed excellent monodispersity, and its size was 5.9 μm (Fig. 2c), but the yield further decreased to 14.9%. When the mass ratio of seed/total monomers was 1 : 2 (**PAD-11**), the particle size of the sphere was 5.4 μm but it was broken, and the adhesion was serious (Fig. 2d), resulting in a low yield of 18.9%. It was hypothesized that the limited amount of seeds could not adequately absorb the monomers, leading to the formation of small particles that adhered to the surface of PAD. Therefore, the polystyrene seeds were increased by 1.5 times (**PAD-10**), which was the best choice. Based on **PAD-9**, the monomer, crosslinker, initiator, aqueous phase and polystyrene seeds were expanded by five times in equal proportions. Although the product (**PAD-12**) displayed spherical morphology and particle size of 7.1 μm (Fig. S3b†), the adhesion was more serious. It was presumed that the change in the reaction conditions, mass transfer problem and the difference of solvent selection in the scale-up experiment may lead to significant differences in the morphology of the microspheres. As depicted in Fig. S3c,† when the amount of the functional monomer to the crosslinker was 1 : 1, the mass ratio of seed/total monomers remained 1 : 3, and **PAD-13** exhibited a spherical shape but was not uniform. Subsequently, when the mass ratio of the seed/total monomers remained at 2 : 5, the resulting **PAD-14** contained a few spheres and most of the irregular particles (Fig. S3d†), whose yield was only 9.5%. Compared with the DBP–toluene system, the morphology of the products fabricated with the toluene–cyclohexanol system was improved but the adhesion of small particles still existed.

**3.1.3 Effect of the binary porogenic system (DBP–cyclohexanol) on the morphologies of PAD.** According to the experiments, it can be deduced that the addition of alcohol had a tremendous effect on the morphology of the product. We tried to select polar DBP and cyclohexanol as the porogenic agent, adjusting the monomer/crosslinker (*n*/*n*), or changing the amount of polystyrene seeds, to further improve the product. When the oil–water volume ratio was maintained at 3 : 50 using DBP and cyclohexanol as porogenic agents, the prepared resin (**PAD-15**) possessed uniform morphology and the particle size

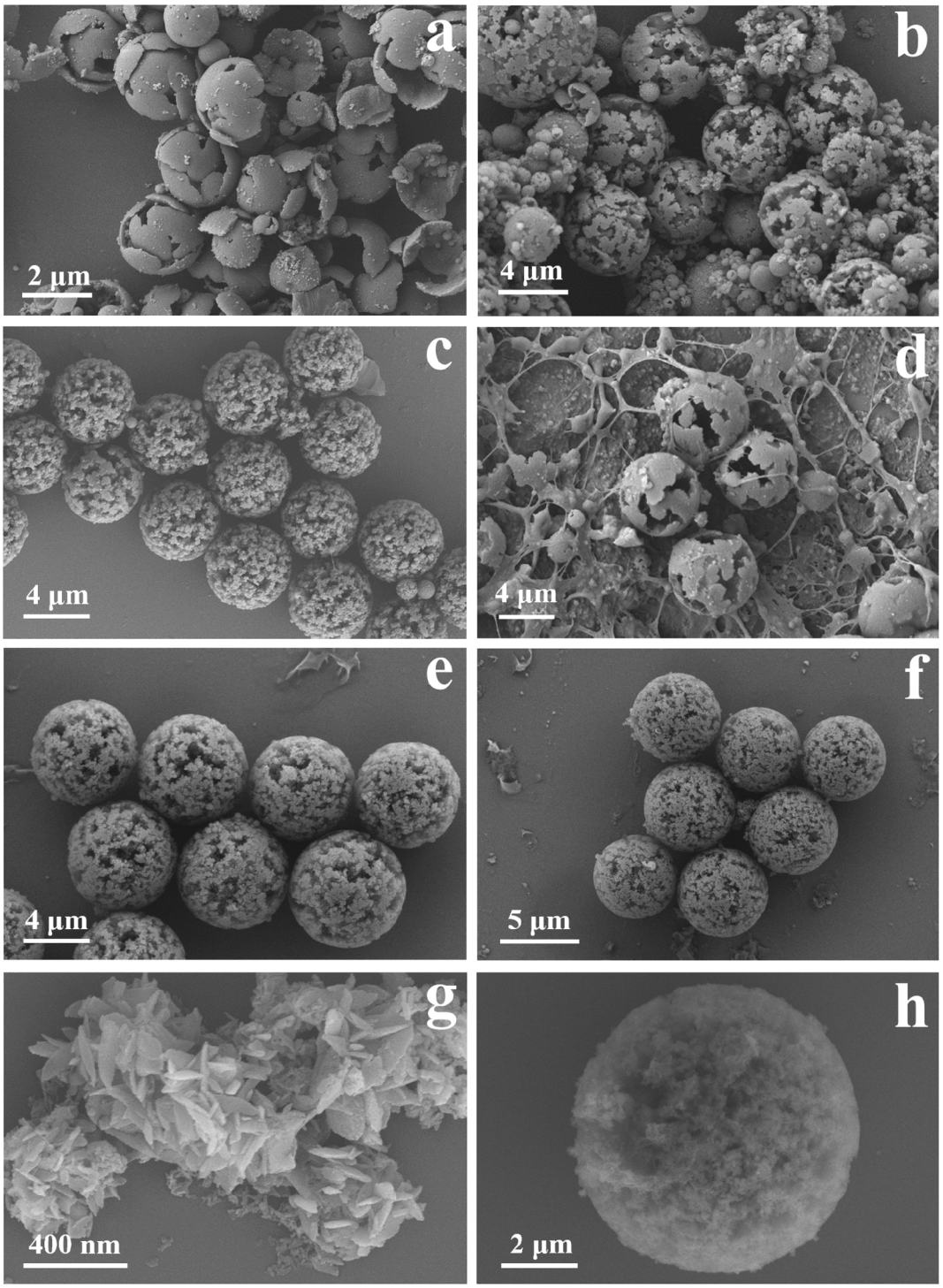


Fig. 2 SEM images of (a) **PAD-1**, (b) **PAD-6**, (c) **PAD-10**, (d) **PAD-11**, (e) **PAD-17**, (f) **PAD-18**, (g) COF and (h) **PAD@COF**.

was 5.1 μm (Fig. S4a†), but a few small particles adhered on its surface, and the yield was 21.4%. Similarly, when the amounts of the monomer, crosslinker, initiator, aqueous phase and polystyrene seeds were expanded by five times in equal proportions (**PAD-16**), the monodisperse microspheres were acquired, the particle size of the microspheres reached 6.2 μm (Fig. S4b†), and the yield was significantly increased to 39.5%. Although the homogeneity and monodisperse of the spheres were significantly improved by the above experimental improvement, the surface of the resin ball was still rough. When the monomer/crosslinker ($n/n$) was 3 : 2 (**PAD-17**), the surface roughness of the microspheres was reduced, the particle size was 6.4 μm (Fig. 2e), and the yield reached 39.2%. When the monomer/crosslinker ($n/n$) was 2 : 1 (**PAD-18**), the surface

 

roughness of the prepared microspheres changed significantly, the particle size of the microspheres was 6.3 μm (Fig. 2f), and the yield was 35.6%. Ultimately, the product **PAD-18** was selected for following modification.

### 3.2 Characterization of materials

As the PAD contains aldehyde groups, it can react with the amino groups of ODH to produce hydrazone bonds. As a result, ODH and Tp were mixed with PAD to coat a layer of two-dimensional COF *via* a "one-pot" method. Fig. 2g depicts the morphology of powdered COF, while Fig. 2h presents the SEM image of **PAD@COF**. Compared with the pristine PAD microspheres, the color is remarkably changed from white to yellow. Additionally, a layer of material appears on the surface of the PAD microsphere, which also proved the successful fabrication of **PAD@COF**.

The FT-IR spectra of PAD, COF and **PAD@COF** are depicted in Fig. 3a. The peak at 1260 $cm^{-1}$ in the PAD spectrum was the stretching vibration peak of =C–O–C, and the stretching vibration peak of C=O was proved at 1731 $cm^{-1}$. In the COF spectrum, the peak at 1681 $cm^{-1}$ is related to the C=O stretching vibration, the peak at 1623 $cm^{-1}$ corresponded to the –C–N stretching vibration, and the vibration peak at 3235 and 3419 $cm^{-1}$ is considered to be the symmetric and asymmetric stretching vibration mode of $-NH_2$ groups in ODH. It is worth noting that in the **PAD@COF** spectrum, the C=O stretching vibration peak at 1683 $cm^{-1}$ corresponded to the stretching vibration peaks of PAD and COF, and the symmetric and asymmetric stretching vibration modes of $-NH_2$ groups at 3236 and 3417 $cm^{-1}$ corresponded to the N–H stretching vibration of ODH in the COF monomer. The appearance of these three characteristic peaks confirmed the successful synthesis of **PAD@COF**.

The elemental composition of PAD and **PAD@COF** was determined by XPS. As presented in Fig. S5a,† the existence of carbon, oxygen and nitrogen elements was detected in **PAD@COF**, while nitrogen element was not observed. Additionally, the elemental analysis of PAD demonstrated that the composition of PAD is primarily comprised of 84.99% carbon and 15.01% oxygen (Table S1†), indicating the absence of nitrogen. **PAD@COF** mainly contains carbon, oxygen and nitrogen elements with contents of 75.64%, 20.72% and 3.65%, respectively. Among them, nitrogen was mainly derived from ODH. For **PAD@COF**, it can be observed from Fig. S5b–d† that the C 1s profile consisted of four fitting peaks, where C=O, C–N, C–O, and C–C were centered at 288.2, 285.8, 285.5 and 284.3 eV,[30] respectively, while the O 1s also consisted of three fitting peaks, *viz.*, O=C, O–H and O–C, centered on 531.3, 532.8 and 532.5 eV, respectively.[31] The N 1s profile of the **PAD@COF** consisted of two fitting peaks, including $-NH_2$ and –N centered on the binding energy of 398.8 and 399.7 eV, respectively.[32] Chemical shifts of C=O, C–O, and O=C were observed in the spectrum of **PAD@COF** compared to PAD, as well as new C–N peaks and N 1s peaks, indicating that the COF was successfully coated onto PAD.

The pore structure and specific surface area pore structure of PAD and **PAD@COF** were analyzed, and the results are listed in

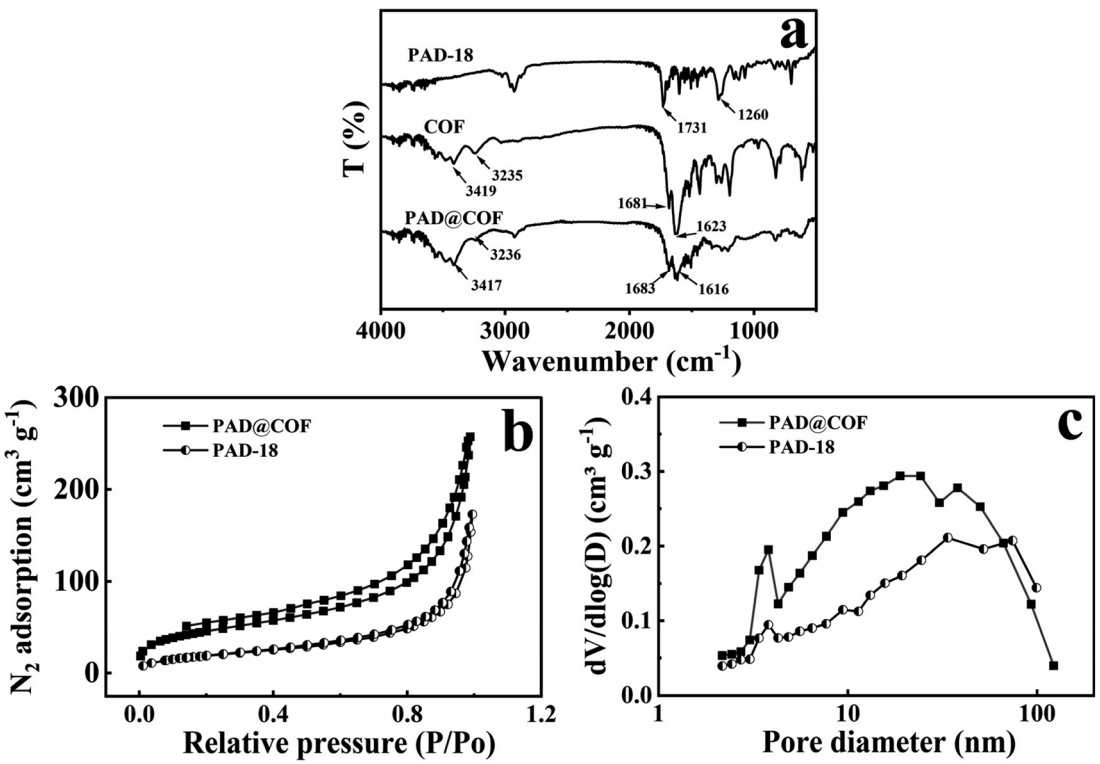


Fig. 3 (a) FT-IR spectra of PAD-18, COF and PAD@COF, (b) nitrogen adsorption isotherms and (c) pore diameter distribution of PAD-18 and PAD@COF.

Table 2. The specific surface area of **PAD-6** synthesized in the DBP-toluene system was measured to be 10.7 $m^2 g^{-1}$, while that of **PAD-11** synthesized in the toluene–cyclohexanol system was measured to be 12.9 $m^2 g^{-1}$. **PAD-15**, **PAD-17**, and **PAD-18** were synthesized using DBP–cyclohexanol as the porogenic agent, resulting in specific surface areas of 26.7, 60.9, and 71.8 $m^2 g^{-1}$, respectively. According to our previous report,[29] the specific surface area of COF was 835 $m^2 g^{-1}$. **PAD-18** was coated with COF to obtain **PAD@COF** with a specific surface area of 163.8 $m^2 g^{-1}$. The BET curves of all the samples in Fig. 3b show a IV-type isotherm pattern based on IUPAC, indicating the existence of mesopores.[33–35] The rapid uptake of nitrogen from 0.8–1.0 was observed, indicating that **PAD@COF** possessed a macroporous structure. All these indicated that the material had a porous structure. The pore volume and specific surface area of **PAD@COF** increased by 35.0% and 56.2%, respectively, compared with **PAD-18**. It was due to the increase in the adsorption pores on the surface of the microspheres after the modification of the COF layer, which also indicated that the COF layer was successfully grafted to the surface of PAD. With the increase in relative pressure, the slope of the curve decreased, and the adsorption from single layer to multi-layer gradually changed.[36] The pore size distribution depicted in Fig. 3c also confirmed the presence of mesopores and macropores within the range of 10–60 nm in the **PAD@COF** material, thereby providing adsorption sites for heavy metals. Furthermore, the existence of these large macropores was conducive to enhancing the mass transfer rate.

### 3.3 Adsorption ability

As presented in Fig. 4a, the adsorption performance of **PAD@COF** can be investigated through isothermal adsorption experiments. When the concentration of $Cu^{2+}$ was less than 20 mg $L^{-1}$, with the increase in $Cu^{2+}$ concentration, the adsorption of $Cu^{2+}$ by **PAD@COF** rapidly increased. When the concentration of $Cu^{2+}$ was about 40 mg $L^{-1}$, the adsorption equilibrium was reached, and the maximum adsorption amount of $Cu^{2+}$ was 270.9 mg $L^{-1}$. The equilibrium adsorption isotherm was fitted through the experimental data, as shown in Table S2 and Fig. S6a–d.† It could be observed that the Langmuir model ($R_L = 0.999$) possessed a higher degree of fitting and correlation coefficient.

Table 2 Specific surface area, pore size, and pore volume of PAD and PAD@COF

| Materials | Specific surface area ($m^2 g^{-1}$) | Pore volume ($cm^3 g^{-1}$) | Average pore diameter (nm) |
|---|---|---|---|
| **PAD-6** | 10.7 | 0.02 | 8.9 |
| **PAD-11** | 12.9 | 0.03 | 7.7 |
| **PAD-15** | 26.7 | 0.19 | 29.4 |
| **PAD-17** | 60.9 | 0.23 | 14.9 |
| **PAD-18** | 71.8 | 0.26 | 14.5 |
| COF | 835 | 0.89 | 15.5 |
| **PAD@COF** | 163.8 | 0.40 | 9.7 |

The experimental results demonstrated that the Langmuir model ($R_L = 0.999$) featured a higher degree of fitting and higher correlation coefficient than that of the Freundlich model ($R_F = 0.932$). The adsorption was chiefly carried out on the surface of **PAD@COF**. During the isothermal adsorption experiment, an increase in $Cu^{2+}$ concentration resulted in a corresponding increase in $Q_e$. This phenomenon can be attributed to the disparity in $Cu^{2+}$ concentration, which consequently led to enhanced mass transfer of $Cu^{2+}$ onto the adsorbent surface.[37]

The kinetic adsorption properties of **PAD@COF** for $Cu^{2+}$ were investigated at 30 mg $L^{-1}$ concentration and different adsorption times. As shown in Fig. 4b, the kinetic adsorption results showed that the adsorption capacity increased rapidly within the initial 50 min and then gradually slowed down, reaching the adsorption equilibrium at about 180 min. The faster first stage could be explained by the fact that abundant binding sites enhance the contact between **PAD@COF** and $Cu^{2+}$, and the adsorption reaction mainly occurs on the surface of the adsorbed material. When the adsorption sites on **PAD@COF** tend to be saturated, the effective adsorption sites are occupied by $Cu^{2+}$, resulting in a slowing down of the increase in the adsorption capacity until equilibrium. The linear regression equation was adopted to fit the adsorption data, as shown in Fig. S6e and f.† The relevant kinetic parameters determined by the pseudo-first-order and pseudo-second-order models are listed in Table S3.† The correlation coefficient ($R_2 = 0.999$) of the pseudo-second-order model was higher than that of the pseudo-first-order ($R_1 = 0.982$). It could be concluded that the experimental data fit the pseudo-second-order model well, which indicated that chemical adsorption mainly occurred on its surface.

The comparison of this kind of microsphere with other materials on the adsorption of $Cu^{2+}$ is exhibited in Table 3. Li and his group prepared a magnetic cellulose nanofiber hydrogel to remove $Cu^{2+}$ from wastewater using cellulose nanofiber materials prepared from agricultural waste soybean residue, poly(vinyl alcohol) with excellent biocompatibility, hydrophilic diatomite, and nano-$Fe_3O_4$. The adsorption equilibrium of magnetic hydrogel reached 720 min and the maximum adsorption capacity was 100 mg $g^{-1}$.[38] Bai *et al.* synthesized spherical $Cu^{2+}$-imprinted polymer using methacrylic acid as the monomer and poly(glycidyl methacrylate-*co*-polyethylene glycol dimethacrylate) as a matrix through atom-transfer radical polymerization. The adsorption equilibrium of the product was reached within 30 min and the maximum adsorption capacity reached 85.6 mg $g^{-1}$.[39] Lu and co-workers adopted surface ion-imprinting technology to selectively adsorb and detect $Cu^{2+}$ in lake water using mesoporous silica-modified rice husk as the carrier and organosilane as the ion-acceptor, and the maximum adsorption capacity was 87.8 mg $g^{-1}$.[40] Zou *et al.* selected cicada shells as raw materials and prepared a porous nitrogen-doped activated biochar by chemical activation treatment, which exhibited excellent electrochemical properties and was applied to manufacture $Cu^{2+}$ sensors, and the maximum adsorption capacity of $Cu^{2+}$ was 110 mg $g^{-1}$.[41] Xu *et al.* collected sludge from a paper mill to prepare sludge-chitosan nanocomposite

 

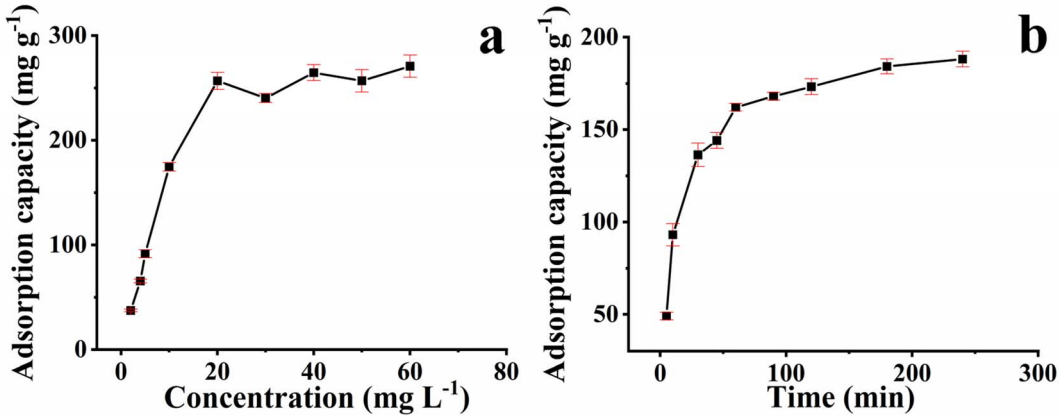


Fig. 4 Adsorption (a) isothermal and (b) kinetic curves of copper ion on PAD@COF.

beads with a maximum adsorption capacity of 115 mg $g^{-1}$ for $Cu^{2+}$.[42] There are also studies using 2,4,6-triformylphloroglucinol and tri(4-aminophenyl)amine as raw materials to successfully synthesize two-dimensional imine-based COF material,[43] which manifested a large specific surface area (686 $m^2$ $g^{-1}$) and also exhibited high sensitivity in the fluorescence test. At pH = 6, the adsorption capacity of $Cu^{2+}$ reached 229 mg $g^{-1}$, which can be utilized as an adsorbent and fluorescence probe for $Cu^{2+}$ removal and detection. Our group previously reported a COF synthetic strategy using flexible alkyl amine as the building unit and intramolecular hydrogen bonding as the network connection.[29] By exploring ODH and Tp, a type of COF material was acquired and its specific surface area was as high as 835 $m^2$ $g^{-1}$, exhibiting a superior adsorption capacity of 324 mg $g^{-1}$.[29] Herein, although the maximum adsorption capacity of **PAD@COF** was marginally lower than that of the hydrazone-linked COF, it exhibited superior adsorption performance compared to other six kinds of $Cu^{2+}$ adsorption materials. Furthermore, **PAD@COF** demonstrated a shorter equilibrium adsorption time in comparison to the magnetic hydrogel, activated carbon and imine-based COF materials.

The reusability of the adsorbent is a crucial factor in practical applications. Multiple cycles of adsorption and desorption can be utilized to evaluate the adsorption performance of the adsorbent and reduce the adsorption cost. The reusability of **PAD@COF** was investigated after 10 cycles of adsorption and desorption experiments. The amounts of adsorption for each cycle were 136.30, 131.45, 130.06, 125.90, 124.51, 123.82, 121.74, 116.19, 112.73, and 107.18 mg $g^{-1}$, respectively. As shown in Fig. 5, the adsorption capacity of **PAD@COF** slightly decreased, but the adsorption efficiency remained over 78.6% after the 10 cycles. It was evident that the washing process has minimal impact on the porous structure and chemical properties of **PAD@COF**. Therefore, **PAD@COF** possessed good cyclic stability and regeneration properties.

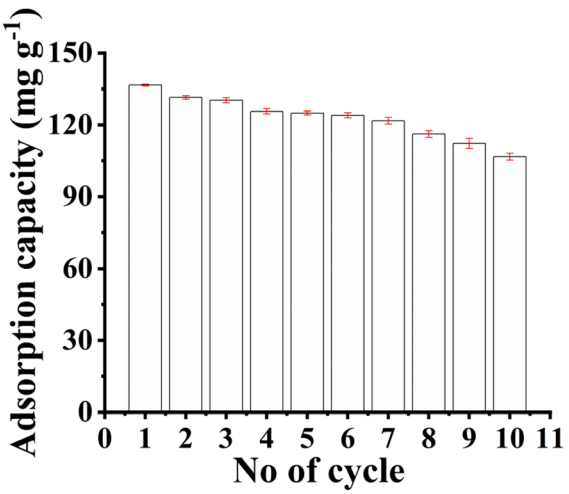


Fig. 5 Reusability of PAD@COF.

Table 3 Comparison of this work with other reported adsorbents for the adsorption of $Cu^{2+}$

| Materials | Maximum adsorption capacity (mg $g^{-1}$) | Equilibrium time (min) | Ref. |
|---|---|---|---|
| TpODH | 324 | 300 | 18 |
| Magnetic hydrogel | 100 | 720 | 28 |
| CD@Cu-IIP | 85.6 | 30 | 29 |
| Cu-IIP | 87.8 | 80 | 30 |
| Activated carbon | 110 | 360 | 31 |
| Sludge-chitosan beads | 115 | 150 | 32 |
| Imine-based COF | 229 | 350 | 33 |
| **PAD@COF** | 270.9 | 180 | This work |

The adsorption ability of **PAD@COF** in real environments was assessed. The adsorption amount of **PAD@COF** for $Cu^{2+}$ was 43.75 mg $g^{-1}$ within 1 h, and the LOD did not change significantly in the lake water sample. This indicated that **PAD@COF** enabled the rapid adsorption of $Cu^{2+}$.

### 3.4 Degradation and recovery

**PAD@COF** was added into different concentrations of acid solution. As shown in Fig. S7,† **PAD@COF** appears similar to the COF as the coating was gradually hydrolyzed with the increase in the concentration, achieving recovery and reuse of the aldehyde-containing microspheres.

## 4 Conclusion

In this work, monodisperse resin microspheres (PAD) with a great quantity of aldehyde groups on the surface were synthesized *via* seed swelling polymerization, and the effect of different porogenic systems on the morphology of the resin microspheres was mainly investigated. Subsequently, PAD was utilized as the matrix, and COF was grafted onto the surface of the microspheres by a simple one-pot method (**PAD@COF**). The obtained **PAD@COF** exhibited controllable particle size and potential for the rapid removal of $Cu^{2+}$ in water. Furthermore, due to the presence of aldehyde groups of the PAD microspheres, it could be reused by a reversible condensation reaction, which presented the extensive integration of other COFs. Additionally, the microspheres are apt to be modified through the Ugi reaction with aldehyde groups. It is optimistically expected that this kind of aldehyde-containing monodisperse microspheres can be utilized as chromatographic stationary phases in the future.

## Data availability

The data are available from the corresponding author on reasonable request.

## Author contributions

Xiaoqiong Wang: conceptualization, data curation, methodology, investigation, software, visualization, and writing – original draft. Qingyan Bai: sample preparation, methodology, and software. Mingjia Yan: validation, and visualization. Yashuai Zhao: investigation and data curation. Shujuan Ma: validation and resources. Chunmiao Bo: supervision. Junjie Ou: project administration, funding acquisition and writing – review & editing.

## Conflicts of interest

No conflict of interest exits in the submission of this manuscript, and manuscript is approved by all authors for publication. I would like to declare on behalf of my co-authors that the work described was original research that has not been published previously, and not under consideration for publication elsewhere, in whole or in part. All the authors listed have approved the manuscript that is enclosed.

## Acknowledgements

Financial support is gratefully acknowledged from the Key research and development program of Ningxia (No. 2022BFE02002), the National Natural Sciences Foundation of Ningxia (No. 2021AAC02017) and the CAS-Weigao Research & Development Program ([2017]-009) to J. Ou.

## Notes and references

1 A. P. Côté, A. I. Benin, N. W. Ockwig, M. O'Keeffe, A. J. Matzger and O. M. Yaghi, *Science*, 2005, **310**, 1166–1170.
2 Z. Xiao, X. Nie, Y. Li, Y. Nie, L. Lu and X. Tian, *ACS Appl. Mater. Interfaces*, 2023, **15**, 9524–9532.
3 D. Xu, Y. Jin, C. Li, Y. Fan, S. Kawi, X. Meng, J. Song and N. Yang, *J. Membr. Sci.*, 2024, **700**, 122678.
4 L. Zhong, C. Wang, J. He, Z. lin, X. Yang, R. Li, S. Zhan, L. Zhao, D. Wu, H. Chen, Z. Tang, C. Zhi and H. Lv, *Adv. Mater.*, 2024, 2314050.
5 L. Li, X. Lv, Y. Xue, H. Shao, G. Zheng and Q. Han, *Angew. Chem., Int. Ed.*, 2024, **63**, e202320218.
6 F. Kong, L. Yue, Z. Yang, G. Sun and J. Chen, *ACS Appl. Mater. Interfaces*, 2021, **13**, 21379–21389.
7 Y. Liu, P. Li, R. Cui, C. Qin, L. Wu, X. Zhang, B. Li, J. Ping, Y. Wang, J. Pan, Y. Ying, D. Li, D. Shi and L. Xu, *Trends Anal. Chem.*, 2024, **174**, 117678.
8 K. Hu, Y. Wang, G. Wang, Y. Wu and Q. He, *Food Chem.*, 2023, **429**, 136801.
9 X. Zhong, Q. Ling, P. Kuang and B. Hu, *Chem. Eng. J.*, 2024, **483**, 149339.
10 S. A, H. R and A. G, *npj Clean Water*, 2024, **7**, 31.
11 R. Sen Gupta, S. Islam, A. Malakar, T. Das and S. Bose, *J. Mater. Chem. A*, 2024, **12**, 19094–19108.
12 J. Wang, A. Hassan, A. Elewa and A. El-Mahdy, *J. Mater. Chem. A*, 2024, **12**, 14005–14021.
13 H. Dong, M. Lu, Y. Wang, H. Tang, D. Wu, X. Sun and F. Zhang, *Appl. Catal., B*, 2022, **303**, 120897.
14 C. Li, M. Gao, X. Sun, H. Tang, H. Dong and F. Zhang, *Appl. Catal., B*, 2020, **266**, 118586.
15 H. Dong, X. Meng, X. Zhang, H. Tang, J. Liu, J. Wang, J. Wei, F. Zhang, L. Bai and X. Sun, *Chem. Eng. J.*, 2020, **379**, 122342.
16 K. Miller, J. Gayle, S. Roy, M. Abdellah, R. Hardian, L. Cseri, P. Demingos, H. Nadella, F. Lee, M. Tripathi, S. Gupta, G. Guo, S. Bhattacharyya, X. Wang, A. Dalton, A. Garg, C. Singh, R. Vajtai, G. Szekely and P. Ajayan, *Small*, 2024, **20**, 2401269.
17 S. Kumar, G. Ignacz and G. Szekely, *Green Chem.*, 2021, **23**, 8932–8939.
18 M. Xie, K. Quan, H. Li, B. Liu, J. Chen, Y. Yu, J. Wang and H. Qiu, *Chem. Commun.*, 2023, **59**, 314–317.
19 H. Long, Y. Deng, Y. Zhang, S. Tang and W. Chen, *Microchem. J.*, 2024, **197**, 109900.
20 J. Tan, S. Namuangruk, W. Kong, N. Kungwan, J. Guo and C. Wang, *Angew. Chem., Int. Ed.*, 2016, **55**, 13979–13984.

21 C. Gao, G. Lin, Z. Lei, Q. Zheng, J. Lin and Z. Lin, *J. Mater. Chem. B*, 2017, **5**, 7496–7503.
22 N. Xu, P. Guo, J. Chen, J. Zhang, B. Wang, S. Xie and L. Yuan, *Talanta*, 2021, **235**, 122754.
23 W. Ma, Q. Zheng, Y. He, G. Li, W. Guo, Z. Lin and L. Zhang, *J. Am. Chem. Soc.*, 2019, **141**, 18271–18277.
24 Y. Su, M. Qin, J. Kong, Q. Zhai, D. Yuan, Z. Liu and Y. Fang, *Adv. Funct. Mater.*, 2024, 2400433.
25 J. Xu, G. Feng, D. Ao, X. Li, M. Li, S. Lei and Y. Wang, *Adv. Mater.*, 2024, 2406256, DOI: **10.1002/adma.202406256**.
26 H. S. Sasmal, A. Kumar Mahato, P. Majumder and R. Banerjee, *J. Am. Chem. Soc.*, 2022, **144**, 11482–11498.
27 Q. Zhu, G. Zhang, L. Zhang, S. Wang, J. Fu, Y. Wang, L. Ma, L. He and G. Tao, *J. Am. Chem. Soc.*, 2023, **145**, 6177–6183.
28 J. Hao, F. Wang, X. Dai, B. Gong and Y. Wei, *Talanta*, 2011, **85**, 482–487.
29 Y. Li, C. Wang, S. Ma, H. Zhang, J. Ou, Y. Wei and M. Ye, *ACS Appl. Mater. Interfaces*, 2019, **11**, 11706–11714.
30 P. Wang, L. Yin, J. Wang, C. Xu, Y. Liang, W. Yao, X. Wang, S. Yu, J. Chen, Y. Sun and X. Wang, *Chem. Eng. J.*, 2017, **326**, 863–874.
31 S. Wan, W. Ding, Y. Wang, J. Wu, Y. Gu and F. He, *Chem. Eng. J.*, 2018, **350**, 1135–1143.
32 K. Zhang, B. Chen, J. Mao, L. Zhu and B. Xing, *Environ. Pollut.*, 2018, **240**, 342–352.
33 N. Gan, Q. Sun, L. Zhao, S. Zhang, Z. Suo, X. Wang and H. Li, *J. Mater. Chem. B*, 2021, **9**, 5628–5635.
34 Y. Dou, N. Liu, X. Zhang, W. Jiang, X. Jiang and L. Yu, *Chem. Eng. J.*, 2023, **463**, 142398.
35 A. V. Narendra Kumar and W. S. Shin, *Chem. Eng. J.*, 2023, **465**, 142922.
36 X. Xie, H. Gao, X. Luo, T. Su, Y. Zhang and Z. Qin, *J. Environ. Chem. Eng.*, 2019, **7**, 103183.
37 J. Dong, Y. Du, R. Duyu, Y. Shang, S. Zhang and R. Han, *Bioresour. Technol. Rep.*, 2019, **6**, 96–102.
38 P. Li, H. Liu, M. Zhou, H. Lei, B. Jian, R. Liu, X. Li, Y. Wang and B. Zhou, *Ind. Crops Prod.*, 2022, **186**, 115257.
39 Q. Bai, C. Huang, S. Ma, B. Gong and J. Ou, *Sep. Purif. Technol.*, 2023, **315**, 123666.
40 X. Lv, H. Hu, L. Yao, L. Deng, X. Liu, L. Yu and H. He, *Spectrochim. Acta, Part A*, 2023, **298**, 122723.
41 J. Zou, J. Liu, Q. Yu, Y. Gao, S. Chen, X. Huang, D. Hu, S. Liu and L. Lu, *Molecules*, 2022, **27**, 4516.
42 K. Xu, L. Li, Z. Huang, Z. Tian and H. Li, *Sci. Total Environ.*, 2022, **846**, 157399.
43 Y. Zhao, Y. Li, W. Chen and X. Jin, *Inorg. Chem.*, 2024, **63**, 1879–1887.